Broad and differential animal ACE2 receptor usage by SARS-CoV-2

Xuesen Zhao[1, 2#]*, Danying Chen[1, 2#], Robert Szabla[3], Mei Zheng[1, 2], Guoli Li[1, 2], Pengcheng Du[1, 2], Shuangli Zheng[1, 2], Xinglin Li[1, 2], Chuan Song[1, 2], Rui Li[1, 2], Ju-Tao Guo[4], Murray Junop[3], Hui Zeng[1, 2]*, Hanxin Lin[5]*

[1]Institute of Infectious disease, Beijing Ditan Hospital, Capital Medical University, Beijing 100015, China.

[2]Beijing Key Laboratory of Emerging Infectious Disease, Beijing 100015, China.

[3]Department of Biochemistry, Western University, 1151 Richmond Street, London, Ontario, Canada.

[4]Baruch S. Blumberg Institute, Hepatitis B Foundation, 3805 Old Easton Road, Doylestown, PA 18902. USA.

[5]Department of Pathology and Laboratory Medicine, Western University, 1151 Richmond Street, London, Ontario, Canada.

Running Title: Broad animal ACE2 receptor usage by SARS-CoV-2

* Corresponding author's e-mail address:

Xuesen Zhao, zhaoxuesen@ccmu.edu.cn

Hui Zeng, zenghui@ccmu.edu.cn

Hanxin Lin, hanxin.lin@lhsc.on.ca

[#] These authors are co-first authors.

ABSTRACT

The COVID-19 pandemic has caused an unprecedented global public health and economy crisis. The origin and emergence of its causal agent, SARS-CoV-2, in the human population remains mysterious, although bat and pangolin were proposed to be the natural reservoirs. Strikingly, comparing to the SARS-CoV-2-like CoVs identified in bats and pangolins, SARS-CoV-2 harbors a polybasic furin cleavage site in its spike (S) glycoprotein. SARS-CoV-2 uses human ACE2 as its receptor to infect cells. Receptor recognition by the S protein is the major determinant of host range, tissue tropism, and pathogenesis of coronaviruses. In an effort to search for the potential intermediate or amplifying animal hosts of SARS-CoV-2, we examined receptor activity of ACE2 from 14 mammal species and found that ACE2 from multiple species can support the infectious entry of lentiviral particles pseudotyped with the wild-type or furin cleavage site deficient S protein of SARS-CoV-2. ACE2 of human/rhesus monkey and rat/mouse exhibited the highest and lowest receptor activity, respectively. Among the remaining species, ACE2 from rabbit and pangolin strongly bound to the S1 subunit of SARS-CoV-2 S protein and efficiently supported the pseudotyped virus infection. These findings have important implications for understanding potential natural reservoirs, zoonotic transmission, human-to-animal transmission, and use of animal models.

Key words: SARS-CoV-2; animal ACE2; receptor; entry; furin cleavage; animal hosts

Introduction

Coronavirus disease 2019 (COVID-19) was first identified in Dec. 2019 in the city of Wuhan, China [1], and has since spread worldwide, causing ~2.3 million infected and around 160,000 fatalities as of April 18th, 2020 (https://coronavirus.jhu.edu/map.html). These numbers are still growing rapidly. The global COVID-19 pandemic has caused an unprecedented public health and economy crisis.

COVID-19 is caused by a novel coronavirus, Severe Acute Respiratory Syndrome Coronavirus 2 (SARS-CoV-2; initially named as 2019-nCoV) [2,3]. The origin of SARS-CoV-2 and its emergence in the human population remain mysterious. Many of the early cases were linked to the Huanan seafood and wild animal market in Wuhan city, raising the possibility of zoonotic origin [4]. Sequencing analyses showed that the genome of SARS-CoV-2 shares 79.5%, 89.1%, 93.3%, and 96.2% nucleotide sequence identity with that of human SARS-CoV, bat coronavirus (CoV) ZC45, bat CoV RmYN02, and bat CoV RaTG13, respectively, suggesting that SARS-CoV-2 probably has bat origins [2,3,5]. This finding is not surprising as bats are notorious for serving as the natural reservoir for many emerging zoonotic viral pathogens, including two other deadly human coronaviruses, SARS-CoV and Middle East respiratory syndrome coronavirus (MERS-CoV), which caused global outbreak during 2002-2003 and 2012-2015, respectively [6,7].

Although SARS-CoV-2 may have originated from bats, bat CoVs are unlikely to jump directly to humans due to the general ecological separation. Other mammal species may have been served as intermediate or amplifying hosts where the progenitor

70 virus acquires critical mutations for efficient zoonotic transmission to human. This has
71 been seen in the emergence of SARS-CoV and MERS-CoV where palm civet and
72 dromedary camel act as the respective intermediate host [7]. The Huanan seafood and
73 wild animal market in Wuhan city would otherwise be a unique place to trace any
74 potential animal source; however, soon after the disease outbreak, the market was
75 closed and all the wild animals were cleared, making this task very challenging or even
76 impossible. As an alternative, wide screening of wild animals becomes imperative.
77 Several recent studies identified multiple SARS-COV-2-like CoVs (SL-CoVs) from
78 smuggled Malayan pangolins in China. These pangolin CoVs (PCoV) form two
79 phylogenetic lineages, PCoV-GX and PCoV-GD [8-11]. In particular, lineage PCoV-GD
80 was found to carry a nearly identical receptor-binding motif (RBM) in the spike (S)
81 protein to that of SARS-CoV-2 (Fig.1). However, the genome of these pangolin
82 SL-CoVs share only 85.5%-92.4% nucleotide identities with that of SARS-CoV-2. This
83 is in contrast to SARS-CoV and MERS-CoV where CoVs isolated form the
84 intermediate host palm civet and dromedary camel share 99.6% and 99.9% % genome
85 sequence identities with their human counterpart, respectively [12,13]. Therefore, pangolins
86 tested in these studies are not the direct intermediate host for SARS-CoV-2. Whether or
87 not SARS-CoV-2 came from other pangolins or other wild animal species remains to be
88 determined.

89 Receptor recognition by the viral S protein is the major determinant of host range,
90 cell, tissue tropism, and pathogenesis of coronaviruses [14]. The S protein of
91 SARS-CoV-2 is a type I membrane glycoprotein, which can be cleaved to S1 and S2
92 subunit during biogenesis at the polybasic furin cleavage site (RRAR) (Fig.1) [15-17].

93 Previous studies have shown that furin cleavage is not essential for coronavirus-cell
94 membrane fusion, but enhances cell-to-cell fusion [18-22], increases the fitness of sequence
95 variant within the quasispecies population of bovine CoV [23], and convert avirulent avian
96 influenza virus isolate to a highly pathogenic isolate [24]. Interestingly, this cleavage site
97 is not present in the S protein of SARS-CoV, bat SL-CoVs or pangolin SL-CoVs
98 identified so far [5,15]. During cell entry, S1 binds to the cellular receptor, subsequently
99 triggering a cascade of events leading to S2-mediated membrane fusion between host
100 cells and coronavirus particles [25]. S1 protein contains an independently folded domain
101 called the receptor binding domain (RBD), which harbors an RBM that is primarily
102 involved in contact with receptor (Fig. 1). Human ACE2 (hACE2) has been identified as
103 the cellular receptor for both SARS-CoV-2 [3,15,17,26] and SARS-CoV [27]. In addition to
104 hACE2, ACE2 from horseshoe bat (*Rhinolophus alcyone*) was found to support cell
105 entry of SARS-CoV-2 S-mediated VSV-based pseudotyped virus [15]. By using infectious
106 virus it has also been shown that ACE2 from Chinese horseshoe bat (*Rhinolophus*
107 *sinicus*), civet and swine, but not mouse, could serve as functional receptors [3]. However,
108 in this infection system, the entry step was coupled with other steps during virus life
109 cycle, i.e. viral genome replication, translation, virion assembly and budding, and thus
110 the receptor activity of these animal ACE2 orthologs were not directly investigated.

111 In an effort to search for potential animal hosts, we examined the receptor activity
112 of ACE2 from 14 mammal species, including human, rhesus monkey, Chinese
113 horseshoe bat (Rs bat), Mexican free-tailed bat (Tb bat), rat, mouse, palm civet, raccoon
114 dog, ferret badger, hog badger, canine, feline, rabbit, and pangolin for SARS-CoV-2 and
115 a mutant virus lacking the furin cleavage site in the S protein. Our results show that

116 multiple animal ACE2 could serve as receptors for SARS-CoV-2 and the SARS-CoV-2
117 mutant. ACE2 of human/rhesus monkey and rat/mouse exhibited the highest and lowest
118 receptor activity, respectively, with the other 10 ACE2s exhibiting intermediate activity.
119 The implications of our findings were discussed in terms of the natural reservoir,
120 zoonotic transmission, human-to-animal transmission, animal health, and animal model.

121 **Results**

122 **Human ACE2 serves as a functional receptor for SARS-CoV-2**

123 To examine the receptor activity of human ACE2 (hACE2) for SARS-CoV-2, we
124 first established a HIV-based pseudotyped virus entry system. This system has been
125 widely used in studies of coronavirus entry. To improve the expression level of S protein
126 and the yield of pseudotyped virus, a codon-optimized S gene based on the sequence of
127 isolate Wuhan-Hu-1 [2] was synthesized and used for production of pseudotyped virus as
128 previously described for other human coronaviruses (HCoVs), including SARS-CoV,
129 MERS-CoV, NL63, 229E, and OC43 [28,29]. The pseudotyped virus was then used to
130 infect 293T cells transfected with either empty vector, or a plasmid expressing APN
131 (receptor for HCoV-229E), DDP4 (receptor for MERS-CoV), ACE1 or hACE2. Two
132 days post-infection, the luciferase activity was measured. As shown in Fig. 2A, only
133 hACE2 was able to efficiently support virus entry. The entry of SARS-CoV-2, but not
134 influenza virus A (IVA) or HCoV-43, was blocked by antibody against hACE2 in a
135 dose-dependent manner (Fig. 2B). We also performed a syncytia formation assay to
136 assess the membrane fusion triggered by hACE2-S binding. As shown in Fig. 1C,
137 syncytia formation was only seen for cells expressing hACE2, but not hACE1, mixed
138 with cells expressing the S protein of SARS-CoV-2 or SARS-CoV. These results

139 confirm that hACE2 is the *bone fide* entry receptor for SARS-CoV-2.

140 **Multiple animal ACE2 orthologs serve as receptors for SARS-CoV-2 and**
141 **SARS-CoV-2 mutant with S protein lacking the furin cleavage site**

142 To test if other animal ACE2 orthologs can also be used as receptor for
143 SARS-CoV-2, we cloned or synthesized ACE2 from rhesus monkey, Chinese horseshoe
144 bat (Rs bat), Mexican free-tailed bat (Tb bat), rat, mouse, palm civet, raccoon dog, ferret
145 badger, hog badger, canine, feline, rabbit, and pangolin. These animals were chosen as
146 being either the proposed natural hosts for SARS-CoV-2 (bat, pangolin) [3,10],
147 intermediate hosts for SARS-CoV (civet, raccoon) [12], common animal model (rat,
148 mouse, monkey), or household pets (canine, feline, rabbit). These ACE2 molecules were
149 transiently expressed in 293T cells (Fig.3A), which were then infected with
150 pseudotyped virus of SARS-CoV-2 (SARS-CoV-2pp). The luciferase activity was
151 measured and normalized to hACE2 (Fig. 3B). The results showed that (1) ACE2 of
152 human and rhesus monkey were the most efficient receptors; (2) ACE2 of rat and mouse
153 barely supported virus entry (<10% of hACE2); (3) the receptor activities of the other
154 10 animal ACE2s were between human/monkey and rat/mouse. Among these, ACE2 of
155 canine, feline, rabbit and pangolin could support virus entry at levels >50% of hACE2.

156 To examine receptor binding ability, we performed immunoprecipitation (IP)
157 analysis by using both S1 and receptor binding domain (RBD) as probe. Among the 14
158 different ACE2s tested, ACE2 from human, monkey, feline, rabbit and pangolin
159 exhibited significant and consistent association with S1 and RBD (Fig.3C). Importantly,
160 these ACE2s correspond to the group of ACE2s that supported the most efficient virus
161 entry (Fig.3B).

162 A striking difference between SARS-CoV-2 and animal SL-CoVs is the presence
163 of a polybasic furin cleavage site at the S1/S2 boundary of the S protein (Fig.1). Here,
164 we generated a SARS-CoV-2 S gene mutant with the furin cleavage site deleted to
165 mimic the bat SL-CoV CZ45. This S mutant has been previously demonstrated to
166 express a full-length non-cleaved S protein during biogenesis in cells [30]. Pseudotyped
167 virus with this mutant S protein was produced and used to infect ACE2-transfected
168 293T cells. Similar or slightly higher efficiency were observed for the mutant S
169 protein-mediated pseudoviral infection in cells transfected with all the animal ACE2s,
170 except for mouse, rat and civet where the mutant S protein mediated a slight lower
171 efficiency of infection. Interesting, pangolin ACE2 was now as efficient as hACE2 for
172 supporting mutant virus entry (Fig.3B).

173 We also tested the receptor usage of these 14 ACE2 by SARS-CoV (Fig.3D). The
174 results indicated that ACE2 of Rs bat and rat were the poorest receptors (<20% of
175 hACE2), while the other ACE2s could support SARS-CoV entry at levels >50% of
176 hACE2. Interestingly, ACE2 of rabbit and pangolin were even more efficient than
177 hACE2 for supporting SARS-CoV entry. Together, these results demonstrated that
178 SARS-CoV-2 and its mutant virus lacking furin cleavage site, as well as SARS-CoV,
179 could use multiple animal ACE2s as receptor.

180 **Molecular basis of different ACE2 receptor activities**

181 To help understand the molecular basis of different ACE2 receptor activities, we
182 first examined the overall sequence variation between these ACE2s. For this purpose,
183 we constructed a phylogenetic tree based on the nucleotide sequences of ACE2s (Fig.4).
184 Interestingly, the phylogenetic clustering of ACE2s is correlated with their abilities to

185 support SARS-CoV-2 entry. For example, ACE2s in subclade IIA (human, rhesus
186 monkey and rabbit) and IIB (rat and mouse) were the most efficient and poorest receptor,
187 respectively, while ACE2s in clade I (from the remaining animals) were intermediate
188 between subclades IIA and IIB. This correlation suggests that sequence variations that
189 define for speciation are responsible for observed differences in receptor activity.

190 Next, based on the published crystal structures of hACE2-RBD complex we
191 compared amino acid sequences of ACE2 receptors, focusing on 23 critical residues in
192 close contact with RBD of SARS-CoV-2 [16,31,32] (Fig. 5). Two obvious patterns were
193 observed. First, hACE2 and rhesus monkey ACE2 are identical at all critical residues
194 for RBD interaction. This explains why rhesus monkey ACE2 supported virus entry as
195 efficient as hACE2 (Fig.3B). Second, since rat and mouse merely support virus entry,
196 the three substitutions (D30N, Y83F and K353H) that are only seen in rat and mouse
197 ACE2s may be the key.

198 To further explain the different receptor activities, we used homology-based
199 structure modeling to analyze the effect of residue substitutions at the atomic level.
200 Structure models of 14 ACE2s were generated based on the crystal structure of
201 SARS-CoV-2 RBD/ACE2 complex [16]. The effects of critical residue substitutions were
202 analyzed and are summarized in Table S1. Overall, the predicted effects of residue
203 substitutions in ACE2s were consistent with corresponding receptor activities. ACE2 of
204 rodents and bats are presented as examples of this analysis (Fig.6).

205 First, we examined the rodent-unique substitutions D30N, Y83F and K353H as
206 they may play a key role in rat and mouse ACE2 inactivity. In humans the residues at
207 all three of these positions directly contact the RBD via hydrogen bonds. D30 contacts

208 K417, Y83 contacts N487, and K353 appears to be at the center of a hydrogen bond
209 network spanning seven RBD residues (Y449, G496, Q498, T500, N501, G502, Y505)
210 and eight ACE2 residues (D38, Y41, Q42, N330, K353, G354, D355, R357). The D30N,
211 Y83F and K353H substitutions are all predicted to disrupt these interactions in rat and
212 mouse ACE2 (Figure 6). This is consistent with previous reports which pinpoint K353
213 as an important hotspot for both SARS-CoV-2 [16] and SARS-CoV [33] binding. It has been
214 experimentally demonstrated that introduction of K353H into hACE2 significantly
215 reduces binding to SARS-CoV S1; in contrast, introduction of H353K into rat ACE2
216 significantly increases binding to SARS-CoV S1 [34]. Our homology models indicate that
217 other residue substitutions may also be contributing to the low viral entry activity in
218 mouse and rat ACE2. Substitutions Q24N, Q27S, M82N, Q325P and E329T in rat
219 ACE2, and L79T, M82S and E329A in mouse ACE2, are all predicted to disrupt
220 interactions with RBD residues (Fig. 6 and Table S1).

221 Both Bat ACE2s are also inefficient receptors for viral entry (Fig.3B). Since the
222 profile of residues at the receptor/RBD interface is significantly different from rat and
223 mouse ACE2, we examined other bat-specific residue substitutions that may be
224 contributing to receptor dysfunction. There are 8 and 10 critical residue substitutions in
225 the Rs bat and Tb bat ACE2s, respectively (Fig.5). Among these, we examined the
226 substitutions at positions Y41, H34 and E329 as they are only seen in bat ACE2s. The
227 Y41H substitution in both bat ACE2s appears to be disrupting the same H-bond network
228 that was disrupted by K353H in rat and mouse ACE2. Although Y41 is not as centrally
229 located in the H-bond network as K353, it directly contacts N501 from the RBD, which is
230 the same residue that is stabilized by K353. A second interaction which appears to be

231 disrupted in only bat ACE2s occurs at position H34. In humans, H34 forms a H-bond
232 with Y453 from the RBD, which is broken through a H34T substitution in bat ACE2s.
233 Finally, the bat-unique substitution E329N appears to be disrupting H-bonds connecting
234 two ACE2 residues (E329, Q325) and two RBD residues (N439, Q506). In Tb bat ACE2,
235 all connections in the H-bond network are disrupted by the single E329N substitution,
236 however the H-bond network is predicted to be restored by an additional substitution,
237 Q325E in Rs bat. In addition, other residue substitutions, i.e. T27M and M82N in Rs bat,
238 and D30Q and L79H in Tb bat, are also disruptive (Fig. 6).

239 These results reveal that the poor and low receptor activity of rodent ACEs and bat
240 ACE2 are resulted from a broken interaction network by a key residue substitution, i.e.
241 K353H in rodents and Y41H in bats, and additive disruptive effects by multiple residue
242 substitutions.

243 **Discussion**

244 In this study, we examined the receptor activity of 14 ACE2 orthologues. The
245 results suggested that wild type and mutant SARS-CoV-2 lacking the furin cleavage site
246 in S protein could use ACE2 from a broad range of animal species to enter host cells.
247 Below we discuss the implication of our findings in terms of natural reservoir, zoonotic
248 transmission, human-to-animal transmission, animal health, and animal model.

249 **Implication in natural reservoirs and zoonotic transmission**

250 Among the 14 ACE2s tested here, hACE2 and rhesus monkey ACE2 are the most
251 efficient receptors, suggesting that SARS-CoV-2 has already been well adapted to
252 humans. In addition, ACE2s of other animals, except mouse and rat, could also support

253 SARS-CoV-2 entry (Fig.3B). Although these data were obtained by using HIV1-based
254 pseudotyped virus, for ACE2 of Rs bat, civet, and mouse, the data is consistent with *in*
255 *vitro* infection data using infectious virus [3]. Receptor usage by coronaviruses has been
256 well known to be a major determinant of host range, tissue tropism, and pathogenesis
257 [14,35,36]. It is therefore reasonable to assume that SARS-CoV-2 would be able to infect all
258 these animals. As a matter of fact, several *in vivo* infection and seroconversion studies
259 have confirmed that SARS-CoV-2 can infect rhesus monkey [37], feline, ferret, and canine
260 [38,39]. Our findings are also in line with the concordance between ACE2 receptor usage
261 by SARS-CoV pseudotyped virus and susceptibility of the animals to SARS-CoV
262 infection. As shown in Fig.3D, ACE2 of rhesus monkey, mouse, civet, ferret badger,
263 raccoon and feline could support SARS-CoV pseudotyped virus entry; concordantly, all
264 these animals are susceptible to native SARS-CoV virus infection [12,40-43].

265 Among all those wild animals that are potentially infected by SARS-CoV-2, bat
266 and pangolin have already been proposed to be the natural reservoirs as closely related
267 SL-CoVs have been identified in bats [2,3,5] and pangolins [8-11]. A recent study has shown
268 that bat SL-CoV RaTG13 could use hACE2 as receptor, consistent with the presence of
269 several favorable hACE2-binding residues (aa 455, 482-486) in the receptor binding
270 motif (RBM) of the S protein (Fig.1) [16]. For pangolin SL-CoVs, lineage PCoV-GD has
271 only one non-critical amino acid substitution (Q483H) in the RBM when compared to
272 SARS-CoV-2 (Fig.1) [10]. Therefore, PCoV-GD most likely can also use hACE2 and
273 other animal ACE2s as functional receptors.

274 We also tested the receptor usage by a SARS-CoV-2 mutant that lacks the furin
275 cleavage site at the S1/S2 boundary. Our result showed that the mutant virus behaved

276 similarly to the wt virus. Namely, the entry of mutant virus could also be supported by
277 those animal ACE2s that supported the entry of wt virus. This result is similar to another
278 study that used the S gene mutant but in a MLV-based pseudotyped virus system [17] and
279 the role of furin cleavage during coronavirus infection. Furin cleavage is not essential
280 for coronavirus-cell membrane fusion, but enhances cell-to-cell fusion [18-21,44]. This
281 could provide certain level of advantage during infection. For example, in the
282 quasispecies population of bovine CoV, a minor sequence variant with a polybasic
283 furin-like cleavage site in the S2 subunit quickly dominated the population even after a
284 single passage in cells [23]. However, by using pseudotyped virus system, which is a
285 single cycle infection system, we may not see the advantage. Still, ours result
286 unequivocally showed that SARS-CoV-2 without this cleavage site could use multiple
287 animal ACE2s as receptors to enter cells. As there is a need to continuously search for
288 potential intermediate hosts for SARS-CoV, results presented here can help significantly
289 narrow down the scope of potential targets.

290 Collectively, our results highlight the potential of these wild animals to serve as
291 natural reservoirs or intermediate hosts for SARS-CoV-2 and its progenitor, the risk of
292 zoonotic transmission of animal SL-CoVs to human, and the necessity of virus
293 surveillance in wild animals.

294 **Implication in human-to-animal transmission and animal health**

295 Among those animal species tested here, canine and feline are of special concern as
296 they are often raised as companion pets. Our data indicate that ACE2 of canine and
297 feline could support SARS-CoV-2 pseudotyped virus entry quite efficiently (>50% of
298 hACE2, Fig.3B), raising the alarming possibility of virus transmission from infected

299 human to these pets or potentially vice versa. As a matter of fact, there was a recent
300 report that a Pomeranian dog in Hong Kong tested weakly positive for SARS-CoV-2
301 while maintaining an asymptomatic state. The genome of the virus isolated from this
302 dog has only three nucleotide changes compared to the virus isolated from two infected
303 persons living in the same household, suggesting that this dog probably acquired the
304 virus from the infected owners [45]. Our results are further supported by two additional
305 studies. One study showed that both dog and cat were susceptible to SARS-CoV-2
306 infection. While the virus replicated poorly in dogs, it replicated efficiently in cats and
307 was able to transmit to unaffected cats that were housed with them [38]. The other study
308 revealed that 14.7% of cat sera samples collected in Wuhan city after the outbreak were
309 positive for antibody against SARS-CoV-2, demonstrating that many cats were infected
310 during the outbreak, most likely from infected humans in close contact [39]. Domestic cats
311 are also susceptible to SARS-CoV infection [40] and human-to-cat transmission was
312 evident during the SARS-CoV outbreak in 2003 in Hong Kong [46]. These findings were
313 also in agreement with our results that ACE2 of cat and dog could serve as receptor for
314 SARS-CoV (Fig.3D).

315 As described above, it seems that dogs are not as susceptible as cats to
316 SARS-CoV-2 [38,45]. Interestingly, this is in agreement with results from IP analysis that
317 showed cat ACE2 could bind to S1 or RBD more efficiently than dog ACE2 (Fig.3C).
318 Structural models further suggest that, at those critical RBD-binding residues, dog and
319 cat ACE2 share 4 substitutions (Q24L, D30E, D38E, and M82T), while dog ACE2 has
320 an additional substitution, H34Y (Fig.5). Based on structural modeling, both Q24L and
321 M82T are predicted to be disruptive, while both D30E and D38E are tolerable (Table

322 S1). H34Y in dog ACE2 is predicted to disrupt the hydrogen bond with Y453 of RBD
323 (Table S1). These atomic interactions explain why dog ACE2 binds to S1 or RBD less
324 efficiently compared to cat ACE2, and both are less efficient than human ACE2.

325 In addition to cat and dog, rabbits are also often raised as household pets. Our
326 results indicate that rabbit ACE2 is an efficient receptor (Fig. 3B and 3C), suggesting
327 that rabbit may be more susceptible to SARS-CoV-2 infection than cat.

328 Currently, there is no evidence that infected pets can transmit the virus back to
329 human; however, this may be possible and should be investigated. Out of an abundance
330 of caution it would be best when one is infected to have both human and pets
331 quarantined, and the pets tested as well.

332 **Implication in animal model**

333 Animal models are essential for study of pathogenesis, vaccinology and
334 therapeutics of viral pathogens. Rodents are probably the most common and amenable
335 animal models because of low cost, easy handling, defined genetics, and the possibility
336 of scalability [47]. However, our results showed that both mouse and rat ACE2 are poor
337 receptors for SARS-CoV-2 (Fig.3B and 3C), suggesting that they are probably resistant
338 to infection. Actually, this has been verified by using infectious SARS-CoV-2 to infect
339 mouse ACE2-transfected cells [3] or mice [48]. Genetically engineered mice expressing
340 hACE2 were previously developed as an animal model for SARS-CoV [49]. This model
341 has been tested recently for SARS-CoV-2, and found to be susceptible to SARS-CoV-2
342 infection and development of interstitial pneumonia [48], a common clinical feature of
343 COVID-19 patients [50]. hACE2-transgenic mice therefore represent useful animal
344 models. However, because of the high demand, and discontinuance due to the

345 disappearance of SARS-CoV in the human population after 2004, it is expected that this
346 mouse model will be in short supply [51]. Alternative methods should be sought to
347 develop a mouse-adapted SARS-CoV-2 strain. Mouse-adapted SARS-CoV strains were
348 developed by serial passage of virus in mice [52,53]. However, this method may not work
349 for SARS-CoV-2 as mouse ACE2 still supports some entry for SARS-CoV (Fig.3D),
350 but not SARS-CoV-2. An alternative way to make a mouse-adapted SARS-CoV-2 strain
351 could be achieved by rational design of the S gene. Based on the structural model, we
352 know that receptor dysfunction of mouse ACE2 is due to disruptive D30N, L79T, M82S,
353 Y83F, E329A and K353H substitutions (Fig.5, Fig.6 and Table S1). Therefore, by
354 specifically introducing mutations into the RBM of S gene it may be possible to restore
355 or at least partly restore interactions with these ACE2 substitutions. Consequently, the
356 engineered virus may be able to efficiently infect wildtype mice.

357 To date, several animals (i.e. rhesus monkey, ferret, dog, cat, pig, chicken and duck)
358 have been examined as potential animal models for SARS-CoV-2 [37,38]. Although the
359 rhesus monkey, ferret and cat may seem to be the promising candidates, none of them
360 are perfect in terms of recapitulation of typical clinical features in COVID-19 patients.
361 Therefore, multiple animal models may be needed. Our results indicate that rabbit
362 ACE2 is a more efficient receptors than other animal ACE2s for both SARS-CoV-2 and
363 SARS-CoV (Fig.3). Therefore, it may be worthy assessing rabbit as a useful animal
364 model for further studies.

365 **Methods**

366 **Cell lines and antibodies**

367 293T cells and Lenti-X 293T cells were cultured in Dulbecco's modified Eagle's

368 medium (DMEM; Gibco) [54]. All growth medium was supplemented with 10% fetal
369 bovine serum (FBS), 110 mg/L sodium pyruvate, and 4.5 g/L D-glucose. β-actin
370 antibody and C9 antibody were purchased from Sigma (A2228) and SANTA CRUZ
371 (sc-57432), respectively. A polyclonal antibody against human ACE2 and anti-IDE
372 polyclonal antibody were purchased from R&D Systems (catalog No. AF933 and
373 AF2496, respectively).

374 **Construction of ACE2 plasmids**

375 ACE2 of human (*Homo sapiens*), civet (*Paguma larvata*), and rat (*Rattus*
376 *norvegicus*) were cloned into a modified pcDNA3.1-cmyc/C9 vector (Invitrogen) as
377 previously described [34,55]. ACE2 protein expressed from this vector has a c-myc tag at
378 the N-terminus and a C9 tag at the C-terminus. An Age I site was engineered right
379 downstream of the signal peptide sequence (nt. 1-54) of ACE2. ACE2 protein expressed
380 from this vector has a c-myc tag at the N-terminus and a C9 tag at the C-terminus.
381 ACE2 of Chinese ferret badger (*Melogale moschata*), raccoon dog (*Nyctereutes*
382 *procyonoides*), Mexican free-tailed bat (*Tadarida brasiliensis*), rhesus monkey (*Macaca*
383 *mulatta*), hog badger (*Arctonyx collaris*), New Zealand white rabbit (*Oryctolagus*
384 *cuniculus*), domestic cat (*Felis catus*) and domestic dog (*Canis lupus familiaris*) were
385 cloned into Age I/Kpn I-digested pcDNA3.1-cmyc-C9 vector previously (Hanxin Lin,
386 Ph. D Thesis Dissertation. "Molecular interaction between the spike protein of human
387 coronavirus NL63 and ACE2 receptor" McMaster University, Health Science
388 Library.https://discovery.mcmaster.ca/iii/encore/record/C__Rb2023203__SMolecular%
389 20interaction%20between%20the%20spike%20protein%20of%20human%20coronavir
390 us%20NL63%20and%20ACE2%20receptor%20Lw%3D%3D%20by%20Hanxin%20Li

391 n__Orightresult__U__X4?lang=eng&suite=def). The nucleotide sequence of ACE2 of
392 Chinese horseshoe bat (*Rhinolophus sinicus*, Rs, GenBank No. KC881004.1) and
393 pangolin (*Manis javanica*, GenBank No. XM_017650263.1) were synthesized and
394 cloned into pcDNA3.1-N-myc/C-C9 vector.

395 **Construction of plasmids expressing S, S1 and RBD of SARS-CoV-2**

396 The nucleotide sequence of SARS-CoV-2 S gene was retrieved from NCBI
397 database (isolate Wuhan-Hu-1, GenBank No. MN908947). According the method
398 described by Gregory J. Babcock et al [56], the codon-optimized S gene was synthesized,
399 and cloned into pCAGGS vector. The SARS-CoV-2 S gene mutant without the furin
400 cleavage site at the S1/S2 boundary was generated by an overlapping PCR-based
401 method as previously described [30]. The S1 subunit (aa 14-685) and RBD (aa 331-524)
402 were cloned into a soluble protein expression vector, pSecTag2/Hygro-Ig vector, which
403 contains human IgG Fc fragment and mouse Ig *k*-chain leader sequence [57]. The protein
404 expressed is soluble and has a human IgG-Fc tag.

405 **Western blot assay**

406 As previously described, the expression of ACE2-C9, S1-Ig, and RBD-Ig fusion
407 proteins were examined by western-blot [57]. Briefly, lysates or culture supernatants of
408 293T cells transfected with plasmid encoding ACE2 orthologs and S1-Ig or RBD-Ig
409 were collected, boiled for 10 min, and then resolved by 4~12% SDS-PAGE. A PVDF
410 membrane containing the proteins transferred from SDS-PAGE was blocked with
411 blocking buffer (5% nonfat dry milk in TBS) for 1h at room temperature and probed
412 with primary antibody overnight at 4 °C. The blot was washed three times with washing
413 buffer (0.05% tween-20 in TBS), followed by incubation with secondary antibody for

414 1h at room temperature. After three-time washes, the proteins bounded with antibodies
415 were imaged with the Li-Cor Odyssey system. (Li-Cor Biotechnology).

416 **Immunoprecipitation (IP) assay.**

417 The association between Ig-fused S1 protein or RBD protein and ACE2 protein
418 with C9 tag was measured by IP according to a previously described method [30]. Briefly,
419 HEK293T cells were transfected with plasmid encoding ACE2 with Lipofectamine
420 2000 (Invitrogen). 48 h post-transfection, the transfected 293T cells were harvested and
421 lysed in PBS buffer containing 0.3 % *n*-decyl-β-D-maltopyranoside (DDM, Anatrace).
422 Cell lysates were incubated with Protein A/G PLUS Agarose (Santa Cruz, sc-2003)
423 together with 4μg of S1-Ig or RBD-Ig. Protein A/G agarose were washed three times in
424 TBS/1% Ttriton-X100, resolved by SDS–PAGE, and detected by western blot using
425 anti-C9 monoclonal antibody.

426 **Production of pseudotyped virus**

427 Following the standard protocol of calcium phosphate transfection, Lenti-X cells in
428 10-cm plate were co-transfected by 20μg of HIV-luc and 10μg of CoVs spike gene
429 plasmid. At 48h post-transfection, 15 ml supernatant was collected and passed through a
430 0.45um pore size PES filter. The purified virus was titrated with Lenti-X p24 Rapid
431 Titer Assay (Takara Bio, Cat. No. 632200). The virus was stored at -80 °C for future
432 use.

433 **Virus entry assay**

434 Each well of 293T cells in a 96-well plate was transfected with 0.1μg of ACE2
435 plasmid DNA following the standard protocol of Lipofectamine 2000 (Invitrogen). At
436 48 hours post-transfection, 150 μl of p24-normalized (10 ng) of pseudotype virus was

437 added into each well and incubated at 37°C for 3 hours. The virus was then removed,
438 and 250 μl of fresh medium was added into each well for further incubation. Two days
439 post-infection, the medium was removed and the cells were lysed with 30 μl/well of 1×
440 cell lysis buffer (Promega) for 15 min, followed by adding 50 μl/well of luciferase
441 substrate (Promega). The firefly luciferase activities were measured by luminometry in
442 a TopCounter (PerkinElmer). For each ACE2, four wells were tested in a single
443 experiment, and at least three repeat experiments were carried out. The luciferase
444 activity was expressed as relative light unit (RLU) and normalized to human ACE2 for
445 plotting.

446 **Syncytial formation assay**

447 293T cells with approximately 90% confluent on 12-well plate were transfected
448 with 1.6μg of plasmid DNA encoding viral S gene or ACE2. At 24 h post-transfection,
449 293T cells expressing the S protein were mixed at a 1:1 ratio with 293T cells expressing
450 ACE2 and plated on 12-well plate. Multinucleated syncytia were observed 24 h after the
451 cells were mixed.

452 **Sequence analysis**

453 Multiple alignments of nucleotide or amino acid sequences of the spike gene of
454 coronaviruses and ACE2 orthologs were performed using Clustal X [58]. Phylogenetic
455 tree was constructed based on the nucleotide sequences of animal ACE2 using the
456 neighbor-joining algorithm implemented in MEGA X. The tree is drawn to scale with
457 branch lengths in the same units as those of the evolutionary distances used to infer the
458 phylogenetic tree. Evaluation of statistical confidence in nodes was based on 1000
459 bootstrap replicates. Branches with <50% bootstrap value were collapsed. Platypus

460 ACE2 (*Ornithorhynchus anatinus*, GenBank No. XM_001515547) was used as an
461 outgroup.

462 **Homology-based structural modeling.**

463 Human ACE2 (PDB: 6VW1) in the bound conformation was extracted from the
464 SARS-CoV-2 RBD/ hACE2 complex and used as a template for homology modeling
465 [16]. ACE2 Homology models were generated using the one-to-one threading algorithm of
466 Phyre2 [59]. The models were then aligned and compared to the intact SARS-CoV-2
467 RBD/ ACE2 complex in PyMOL (The PyMOL Molecular Graphics System, Version 2.0
468 Schrödinger, LLC).

469

470 **FUNDING**

471 This work was supported by grants from the National Natural Science Foundation of
472 China (81772173 and 81971916) and National Science and Technology Mega-Project of
473 China (2018ZX10301-408-002) to X Zhao and from the Canadian Institutes of Health
474 Research (MOP-89903 to MSJ).

475

476

477

478

479

480

481 **Figure and Figure legends**

482

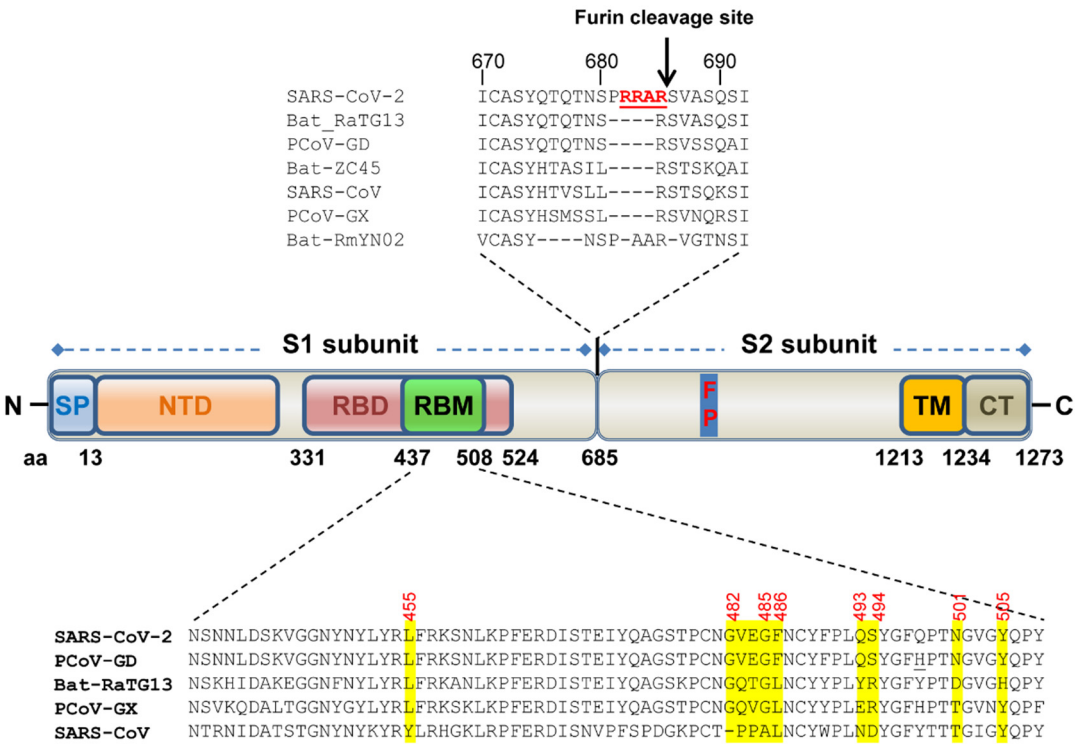

483

484

485 **Fig. 1. Schematic diagram of domain structures and critical ACE2-binding**
486 **residues of the spike (S) protein of SARS-CoV-2.** Signal: signal peptide. NTD: N-
487 terminal domain. RBD: receptor-binding domain. RBM: receptor-binding motif. FP:
488 fusion peptide. TM: transmembrane domain. CT: cytoplasmic tail. The S protein is
489 cleaved into S1 and S2 subunit during biogenesis at the polybasic furin cleavage site
490 (RRAR↓), which is not present in SARS-CoV and other animal SARS-CoV-2-like
491 CoVs. The S1 subunit is required for binding to ACE2 receptor, while the S2 subunit
492 containing a FP mediates membrane fusion. In SARS-CoV-2, the S1 contains NTD and
493 an independently folded domain known as RBD, which harbors a region called receptor
494 binding motif (RBM), that are primarily in contact with receptor. The most critical
495 hACE2-binding residues in the RBM of several SARS-CoV-2-related CoVs are
496 highlighted in yellow and referred from the crystal structure of RBD-hACE2 complex
497 (Shang et al, Nature). PCoV-GX: pangolin CoV isolate GX-PL4. PCoV-GD: pangolin
498 CoV isolate MP789. The only difference in the RBM between PCoV-GD and
499 SARS-CoV-2 is Q498H (underlined). The GenBank No. for these CoVs is:
500 SARS-CoV-2 (isolate Wuhan-Hu-1, MN908947), SARS-CoV (isolate Tor2,
501 NC_004718.3), bat-ZC45 (MG772933.1), bat-RaTG13 (MN996532.1), PCoV-GX
502 (isolate P4L, MT040333.1), PCoV-GD (isolate MP789, MT084071.1).

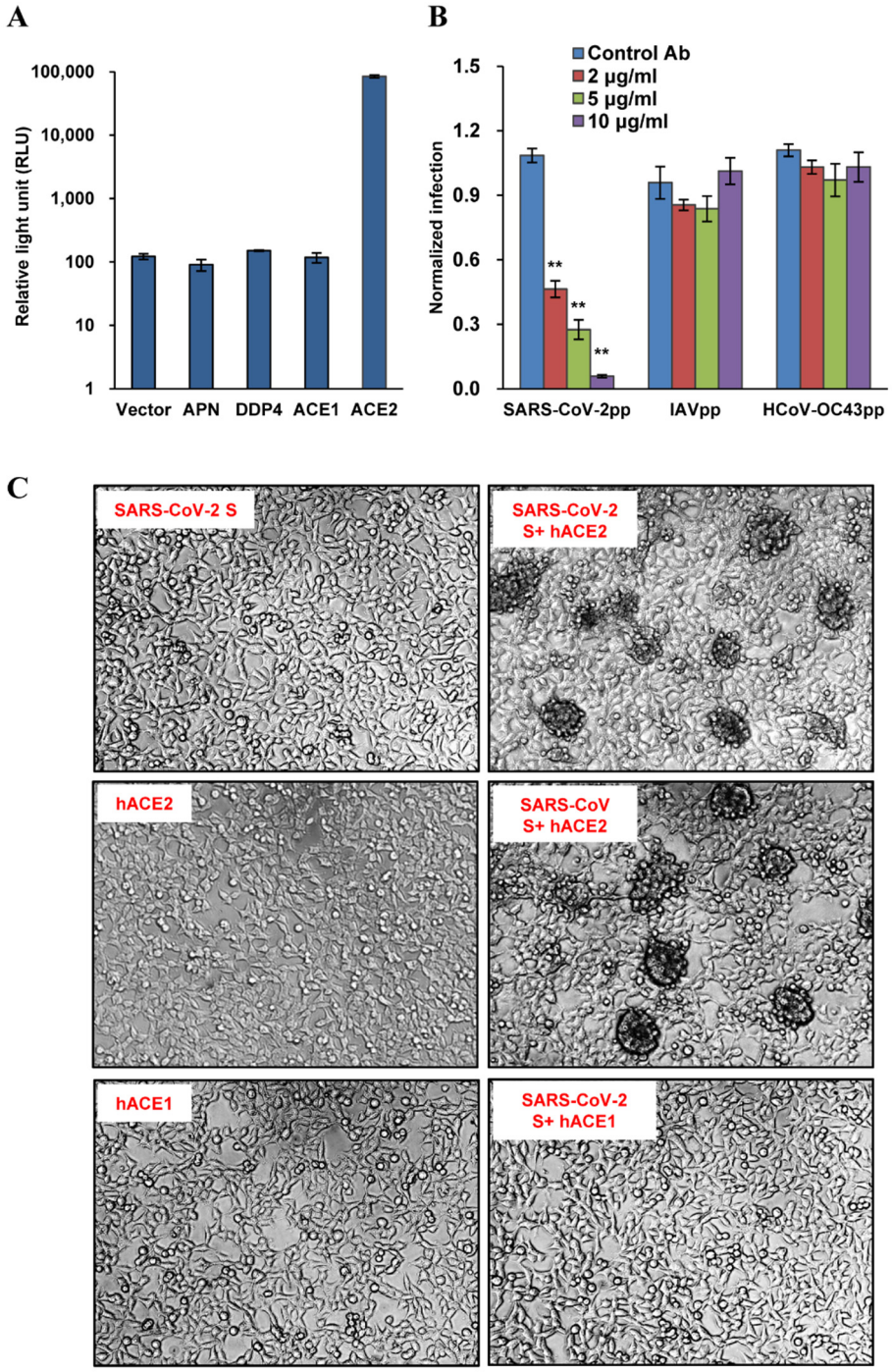

Fig. 2. Human ACE2 served as receptor for SARS-CoV-2. (A) ACE2 supported HIV-Luc-based pseudotyped virus entry. 293T cells were transfected with empty vector pcDNA3.1, APN (receptor for HCoV-229E), DDP4 (receptor for MERS-CoV), ACE1 or ACE2. At 48 h post transfection, the cells were infected by SARS-CoV-2 S protein pseudotyped virus (SARS-CoV-2pp). At 48 h post infection, luciferase activity was measured. (B) Human ACE2 antibody inhibited virus entry at a dose-dependent manner. 293T cells were transfected with ACE2. At 48 h post transfection, the cells were pre-incubated with indicated concentration of hACE2 antibody or control antibody

513 (anti-IDE) for 1 h, and then infected by pseudotyped virus of SARS-CoV-2, Influenza
514 virus A (IAVpp) or human coronavirus (HCoV) OC43 (HCoV-OC43pp) in the presence
515 of indicated concentration of hACE2 antibody or control antibody (anti-IDE) for
516 another 3 h, then the virus and antibodies were removed. At 48 h post infection,
517 luciferase activity was measured and normalized to the control antibody for
518 SARS-CoV-2pp. Error bars reveal the standard deviation of the means from four
519 biological repeats. (C) Syncytia formation assay. 293T cells transfected with a plasmid
520 the expressing S protein of SARS-CoV-2 or SARS-CoV were mixed at a 1:1 ratio with
521 those cells transfected with a plasmid expressing ACE1 or ACE2. Twenty-four hours
522 later, syncytia formation was recorded.

523

524

525

526

527

528

529

530

531

532

533

534

535

536

537

538

539

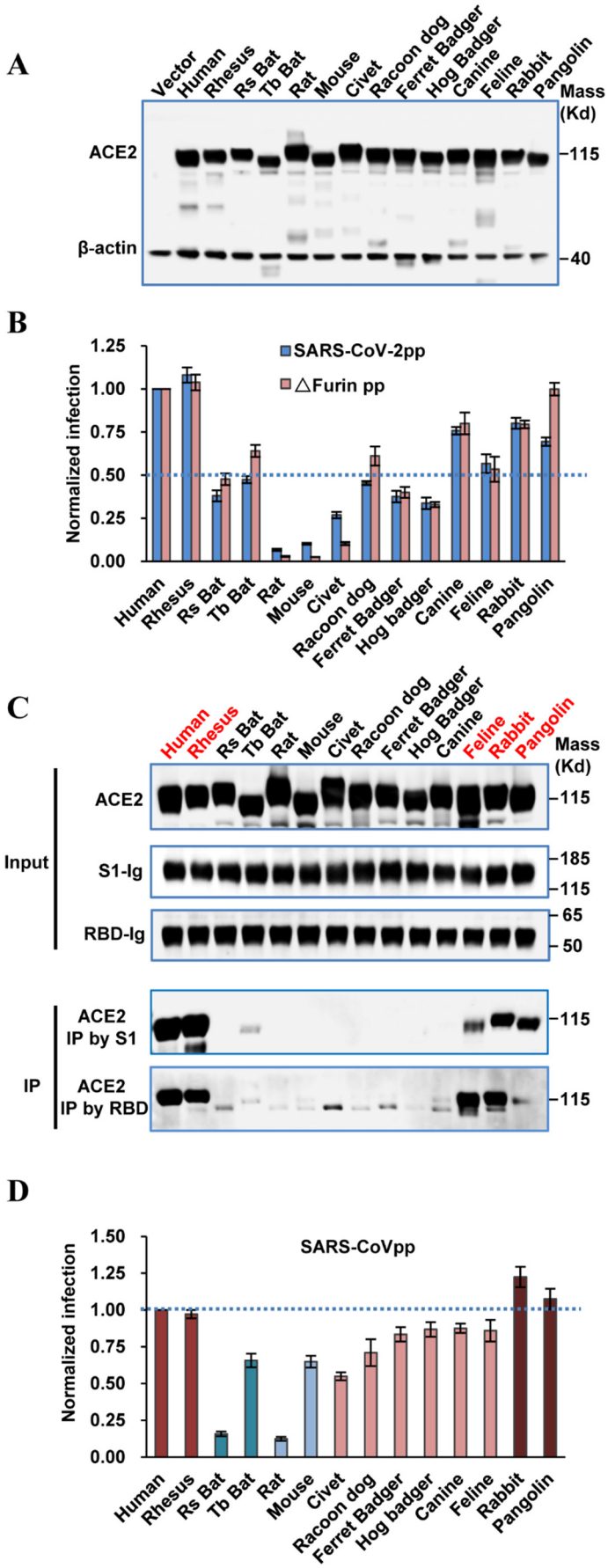

Fig. 3. Multiple ACE2 orthologues served as receptors for SARS-CoV-2. (A) Transient expression of ACE2 orthologs in 293T cells. The cell lysates were detected by western blot assay, using an anti-C9 monoclonal antibody. (B) HIV-Luc-based pseudotyped virus entry. 293T cells were transfected with ACE2s orthologs. At 48 h post transfection, the cells were infected by the pseudotyped virus of wildtype SARS-CoV-2 or mutant ΔFurin. At 48 h post infection, luciferase activity was measured and normalized to human ACE2, respectively. Error bars reveal the standard deviation of the means from four biological repeats. (C) IP assay. The upper panel showed the input of ACE2 protein with C9 tag, S1 and RBD with IgG tag. The lower panel showed the ACE2 pulled down by S1-Ig or RBD-Ig fusion protein.

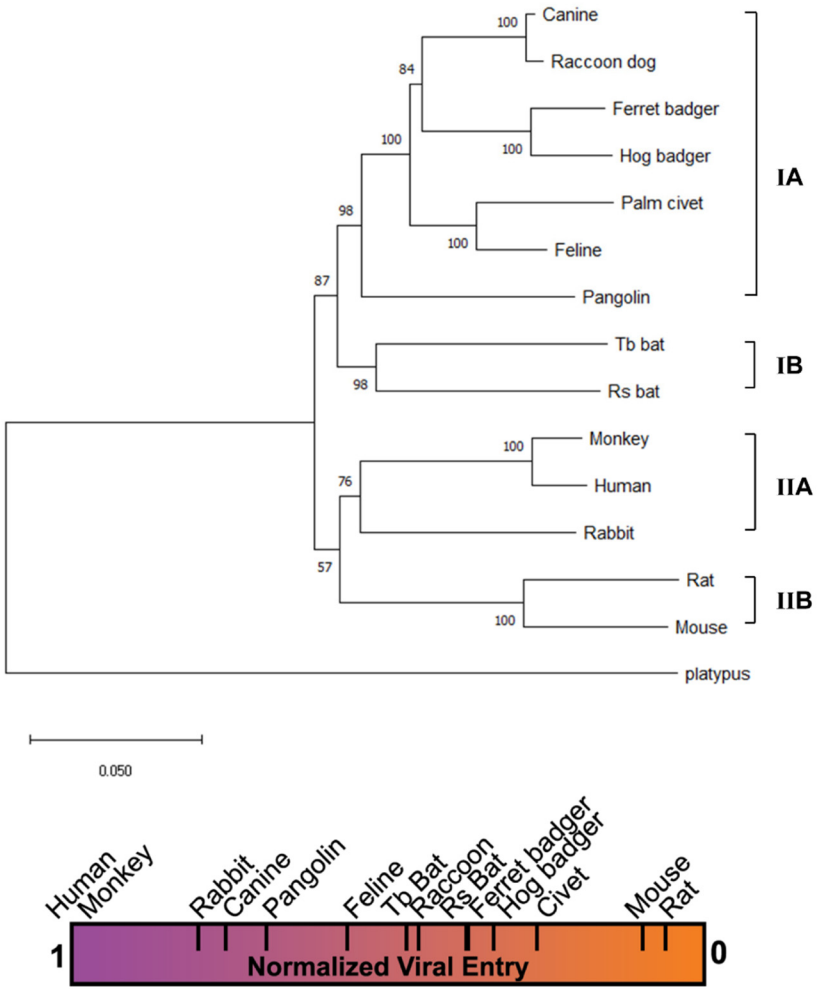

575

576

577

578

579 **Fig. 4. Phylogenetic clustering of ACE2s correlates with their receptor activities.**
580 **Upper panel**: phylogram tree of 14 ACE2s. The tree was constructed based on
581 nucleotide sequences using the Neighbor-joining method implemented in program
582 MEGA X. The percentage of replicate trees in which the associated taxa clustered
583 together in the bootstrap test (1000 replicates) are shown next to the branches. The tree
584 was rooted by ACE2 of platypus (*Ornithorhynchus anatinus*). The taxonomic orders
585 where these animals are classified are shown on the right-hand side of the tree. **Lower**
586 **panel**: a heat bar summarizing the relative levels of pseudotyped virus entry supported
587 by different animal ACE2s.

588

589

590

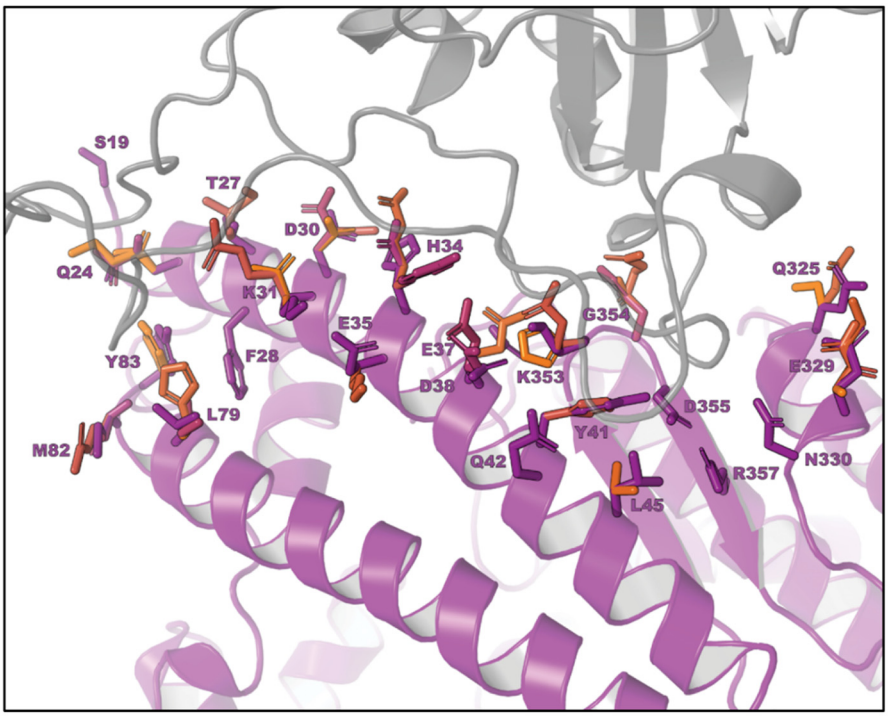

ACE2	19	24	27	28	30	31	34	35	37	38	41	42	45	79	82	83	325	329	330	353	354	355	357
Human	S	Q	T	F	D	K	H	E	E	D	Y	Q	L	L	M	Y	Q	E	N	K	G	D	R
Monkey	-	-	-	-	-	-	-	-	-	-	-	-	-	-	-	-	-	-	-	-	-	-	-
Rs bat	-	E	M	-	-	-	T	K	-	-	H	-	-	-	N	-	E	N	-	-	-	-	-
Tb bat	-	E	I	-	Q	R	T	-	-	E	H	-	-	H	R	-	-	N	-	-	-	-	-
Rat	-	K	S	-	N	-	Q	-	-	-	-	-	-	I	N	F	P	T	-	H	-	-	-
Mouse	-	N	-	-	N	N	Q	-	-	-	-	-	-	T	S	F	-	A	-	H	-	-	-
Civet	-	L	-	-	E	T	Y	-	Q	E	-	-	V	-	T	-	-	-	-	-	D	-	-
Raccoon	-	L	-	-	E	-	Y	-	-	E	-	-	-	-	T	-	-	-	-	R	-	-	-
Ferret badger	-	L	-	-	E	-	-	-	-	E	-	-	-	H	T	-	E	Q	-	-	R	-	-
Hog badger	-	L	-	-	E	-	R	-	-	E	-	-	-	H	T	-	E	K	-	-	H	-	-
Canine	-	L	-	-	E	-	Y	-	-	E	-	-	-	-	T	-	-	-	-	-	-	-	-
Feline	-	L	-	-	E	-	-	-	-	E	-	-	-	-	T	-	-	-	-	-	-	-	-
Rabbit	-	L	-	-	E	-	Q	-	-	-	-	-	-	-	T	-	-	-	-	-	-	-	-
Pangolin	-	E	-	-	E	-	S	-	-	E	-	-	-	I	N	-	-	-	-	-	H	-	-

Fig. 5. Critical RBD-binding residues in ACE2 orthologs. Upper panel: 23 RBD-binding residues at the contact interface between hACE2 and RBD of SARS-CoV-2. Human ACE2 (PDB: 6VW1) in the bound conformation was extracted from the SARS-CoV-2 RBD/ACE2 complex and used as a template for homology modeling [16]. **Low panel**: Critical RBD-binding residues in ACE2 orthologs. Residue substitutions highlighted in red and orange are those unique to both mouse and rat ACE2s and both bats, respectively. The rest of residue substitutions are highlighted in yellow.

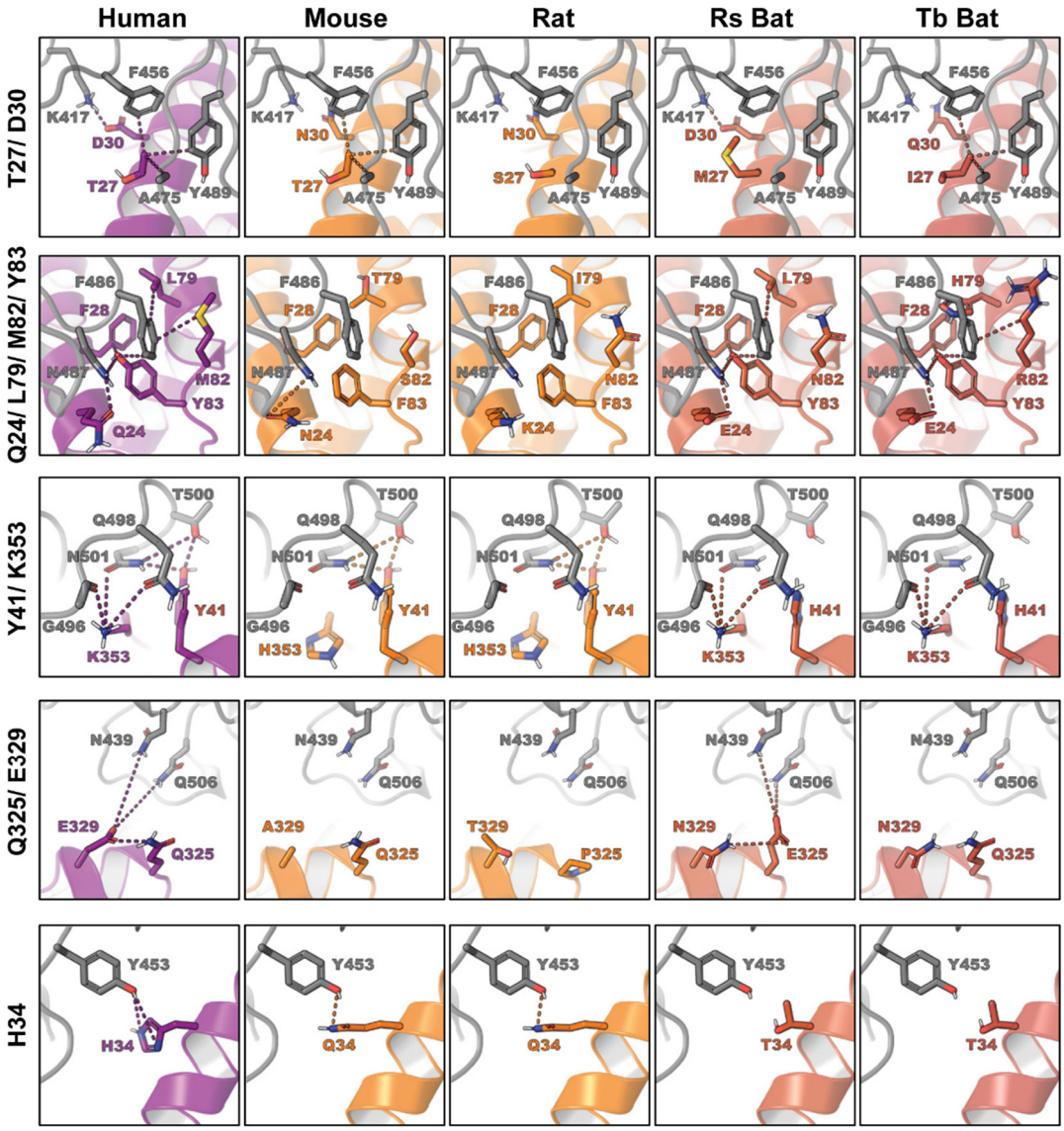

Fig. 6. Structural models of key residue substitutions in ACE2 of mouse, rat and bats. Human ACE2 (PDB: 6VW1) in the bound conformation was extracted from the SARS-CoV-2 RBD/ACE2 complex and used as a template for homology modeling [16]. ACE2 Homology models were generated using the one-to-one threading algorithm of Phyre2 [59]. The models were then aligned and compared to the intact SARS-CoV-2 RBD/ ACE2 complex in PyMOL.

Table S1. Predicted effect of clinical residue substitutions in ACE2 orthologs on the interaction with RBD of SARS-CoV-2

Human ACE2		Interaction			Predicted status of interaction in ACE2 homologs (Disrupted/ Enhanced/ Tolerated/ Unsure/ No residue change)												
Index	Residue	Molecule	Residue	Type	Monkey	BatRs	BatTb	Rat	Mouse	Civet	Raccoon	Ferret	HogBadger	Dog	Cat	Rabbit	Pangolin
19	S	ACE2	Q24	H-bond	-	-	-	-	-	-	-	-	-	-	-	-	-
24	Q	RBD	N487	H-bond	-	T	T	D	T	D	D	D	D	D	D	D	T
		ACE2	S12	H-bond	-	D	D	T	T	D	D	D	D	D	D	D	D
27	T	RBD	Y489	VdW	-	D	T	D	-	-	-	-	-	-	-	-	-
		RBD	A475	VdW	-	D	T	D	-	-	-	-	-	-	-	-	-
		RBD	F456	VdW	-	D	T	D	-	-	-	-	-	-	-	-	-
28	F	ACE2	Y83	π	-	-	-	-	-	-	-	-	-	-	-	-	-
30	D	RBD	K417	H-bond	-	-	D	D	D	T	T	T	T	T	T	T	T
31	K	RBD	Q493	H-bond	-	-	T	-	D	D	-	-	-	-	-	-	-
34	H	RBD	Y453	H-bond	-	D	D	T	T	D	D	-	T	D	-	T	D
35	E	RBD	Q493	H-bond	-	-	-	-	-	-	-	-	-	-	-	-	-
37	E	ACE2	R393	H-bond	-	-	-	-	-	D	-	-	-	-	-	-	-
		RBD	Y505	VdW	-	-	-	-	-	E	-	-	-	-	-	-	-
38	D	ACE2	Q42	H-bond	-	-	-	-	-	T	T	T	T	T	T	-	T
		ACE2	K353	H-bond	-	-	-	-	-	T	T	T	T	T	T	-	T
		RBD	Q498	H-bond	-	-	-	-	-	T	T	T	T	T	T	-	T
		RBD	Y449	VdW	-	-	-	-	-	T	T	T	T	T	T	-	T
41	Y	RBD	Q498	π	-	D	D	-	-	-	-	-	-	-	-	-	-
		RBD	T500	VdW	-	D	D	-	-	-	-	-	-	-	-	-	-
		RBD	N501	H-bond	-	D	D	-	-	-	-	-	-	-	-	-	-
		ACE2	R357	H-bond	-	D	D	-	-	-	-	-	-	-	-	-	-
		ACE2	K353	π	-	D	D	-	-	-	-	-	-	-	-	-	-
42	Q	RBD	Y449	H-bond	-	-	-	-	-	-	-	-	-	-	-	-	-
		ACE2	D38	H-bond	-	-	-	-	-	-	-	-	-	-	-	-	-
45	L	RBD	Q498	VdW	-	-	-	-	-	T	-	-	-	-	-	-	-
79	L	RBD	F486	Hydrophobic	-	-	D	T	D	-	-	D	D	-	-	-	T
82	M	RBD	F486	π	-	D	U	D	D	D	D	D	D	D	D	D	D
83	Y	RBD	F486	π	-	-	-	D	D	-	-	-	-	-	-	-	-
		RBD	N487	H-bond	-	-	-	D	D	-	-	-	-	-	-	-	-
		ACE2	F28	π	-	-	-	D	D	-	-	-	-	-	-	-	-
325	Q	ACE2	E329	H-bond	-	T	D	D	D	-	-	T	T	-	-	-	-
329	E	RBD	Q506	H-bond	-	T	D	D	D	-	-	T	T	-	-	-	-
		RBD	N439	H-bond	-	T	D	D	D	-	-	T	T	-	-	-	-
		ACE2	Q325	H-bond	-	T	D	D	D	-	-	T	T	-	-	-	-
330	N	ACE2	R357	H-bond	-	-	-	-	-	-	-	-	-	-	-	-	-
		ACE2	D355	H-bond	-	-	-	-	-	-	-	-	-	-	-	-	-
353	K	RBD	G496	H-bond	-	-	-	D	D	-	T	-	-	-	-	-	-
		RBD	G502	H-bond	-	-	-	T	T	-	T	-	-	-	-	-	-
		RBD	Y505	π	-	-	-	D	D	-	T	-	-	-	-	-	-
		RDB	Q498	H-bond	-	-	-	D	D	-	T	-	-	-	-	-	-
		RBD	N501	H-bond	-	-	-	D	D	-	T	-	-	-	-	-	-
		ACE2	D38	H-bond	-	-	-	D	D	-	T	-	-	-	-	-	-
		ACE2	Y41	π	-	-	-	T	T	-	T	-	-	-	-	-	-
354	G	RBD	G502	H-bond	-	-	-	-	-	T	-	T	T	-	-	-	T
355	D	RBD	T500	H-bond	-	-	-	-	-	-	-	-	-	-	-	-	-
		ACE2	N330	H-bond	-	-	-	-	-	-	-	-	-	-	-	-	-
		ACE2	R357	H-bond	-	-	-	-	-	-	-	-	-	-	-	-	-
357	R	RBD	T500	H-bond	-	-	-	-	-	-	-	-	-	-	-	-	-
		ACE2	N330	H-bond	-	-	-	-	-	-	-	-	-	-	-	-	-
		ACE2	Y41	H-bond	-	-	-	-	-	-	-	-	-	-	-	-	-
		ACE2	D355	H-bond	-	-	-	-	-	-	-	-	-	-	-	-	-

H-bond: hydrogen bond; Vdw: Van der Waals force; D: disruptive; T: tolerated; U: unsure; E: enhanced.

The effects of residues substitution were predicted by homologous-based modeling analyses based on the crystal structure of SARS-CoV-2 RBD/hACE2 complex (Ref.16)

References

1 Zhu, N. *et al.* A Novel Coronavirus from Patients with Pneumonia in China, 2019. *N Engl J Med* **382**, 727-733, doi:10.1056/NEJMoa2001017 (2020).

2 Wu, F. *et al.* A new coronavirus associated with human respiratory disease in China. *Nature* **579**, 265-269, doi:10.1038/s41586-020-2008-3 (2020).

3 Zhou, P. *et al.* A pneumonia outbreak associated with a new coronavirus of probable bat origin. *Nature* **579**, 270-273, doi:10.1038/s41586-020-2012-7 (2020).

4 Lu, R. *et al.* Genomic characterisation and epidemiology of 2019 novel coronavirus: implications for virus origins and receptor binding. *Lancet* **395**, 565-574, doi:10.1016/S0140-6736(20)30251-8 (2020).

5 Hong Zhou, X. C., Tao Hu, Juan Li, Hao Song, Yanran Liu, Peihan Wang, Di Liu, Jing Yang, Edward C. Holmes, Alice C. Hughes, Yuhai Bi, Weifeng Shi. A novel bat coronavirus reveals natural insertions at the S1/S2 cleavage site of the Spike protein and a possible recombinant origin of HCoV-19. *BioRxiv* **https://doi.org/10.1101/2020.03.02.974139** (2020).

6 Hayman, D. T. Bats as Viral Reservoirs. *Annu Rev Virol* **3**, 77-99, doi:10.1146/annurev-virology-110615-042203 (2016).

7 Cui, J., Li, F. & Shi, Z. L. Origin and evolution of pathogenic coronaviruses. *Nat Rev Microbiol* **17**, 181-192, doi:10.1038/s41579-018-0118-9 (2019).

8 Zhang, T., Wu, Q. & Zhang, Z. Probable Pangolin Origin of SARS-CoV-2 Associated with the COVID-19 Outbreak. *Curr Biol*, S0960-9822(0920)30360-30362, doi:10.1016/j.cub.2020.03.022 (2020).

9 Xiao, K. P. *et al.* Isolation and Characterization of 2019-nCoV-like Coronavirus from Malayan Pangolins. *BioRxiv* **https://doi.org/10.1101/2020.02.17.951335**, doi:https://doi.org/10.1101/2020.02.17.951335 (2020).

10 Lam, T. T.-Y. *et al.* Identifying SARS-CoV-2 related coronaviruses in Malayan pangolins. *Nature* **https://doi.org/10.1101/2020.02.13.945485**, doi:https://doi.org/10.1101/2020.02.13.945485 (2020).

11 Liu, P., Chen, W. & Chen, J. P. Viral Metagenomics Revealed Sendai Virus and Coronavirus Infection of Malayan Pangolins (Manis javanica). *Viruses* **11**, doi:10.3390/v11110979 (2019).

12 Guan, Y. *et al.* Isolation and characterization of viruses related to the SARS coronavirus from animals in southern China. *Science* **302**, 276-278 (2003).

13 Hemida, M. G. *et al.* MERS coronavirus in dromedary camel herd, Saudi Arabia. *Emerg Infect Dis* **20**, 1231-1234, doi:10.3201/eid2007.140571 (2014).

14 Li, F. Receptor recognition and cross-species infections of SARS coronavirus. *Antiviral Res* **100**, 246-254, doi:10.1016/j.antiviral.2013.08.014 (2013).

15 Hoffmann, M. *et al.* SARS-CoV-2 Cell Entry Depends on ACE2 and TMPRSS2 and Is Blocked by a Clinically Proven Protease Inhibitor. *Cell* **10.1016/j.cell.2020.02.052**, doi:10.1016/j.cell.2020.02.052 (2020).

16 Shang, J. *et al.* Structural basis of receptor recognition by SARS-CoV-2. *Nature* **10.1038/s41586-020-2179-y**, doi:10.1038/s41586-020-2179-y (2020).

670 17 Walls, A. C. *et al.* Structure, Function, and Antigenicity of the SARS-CoV-2 Spike Glycoprotein.
671 *Cell* **10.1016/j.cell.2020.02.058**, doi:10.1016/j.cell.2020.02.058 (2020).
672 18 Bos, E. C., Heijnen, L., Luytjes, W. & Spaan, W. J. Mutational analysis of the murine
673 coronavirus spike protein: effect on cell-to-cell fusion. *Virology* **214**, 453-463,
674 doi:S0042-6822(85)70056-6 [pii]
675 10.1006/viro.1995.0056 (1995).
676 19 de Haan, C. A., Stadler, K., Godeke, G. J., Bosch, B. J. & Rottier, P. J. Cleavage inhibition of the
677 murine coronavirus spike protein by a furin-like enzyme affects cell-cell but not virus-cell fusion.
678 *J Virol* **78**, 6048-6054, doi:10.1128/JVI.78.11.6048-6054.2004
679 78/11/6048 [pii] (2004).
680 20 Stauber, R., Pfleiderera, M. & Siddell, S. Proteolytic cleavage of the murine coronavirus surface
681 glycoprotein is not required for fusion activity. *J Gen Virol* **74 (Pt 2)**, 183-191 (1993).
682 21 Taguchi, F. Fusion formation by the uncleaved spike protein of murine coronavirus JHMV
683 variant cl-2. *J Virol* **67**, 1195-1202 (1993).
684 22 Millet, J. K. & Whittaker, G. R. Host cell proteases: Critical determinants of coronavirus tropism
685 and pathogenesis. *Virus Res* **202**, 120-134, doi:10.1016/j.virusres.2014.11.021 (2015).
686 23 Borucki, M. K. *et al.* The role of viral population diversity in adaptation of bovine coronavirus to
687 new host environments. *PLoS One* **8**, e52752, doi:10.1371/journal.pone.0052752 (2013).
688 24 Ito, T. *et al.* Generation of a highly pathogenic avian influenza A virus from an avirulent field
689 isolate by passaging in chickens. *Journal of virology* **75**, 4439-4443,
690 doi:10.1128/JVI.75.9.4439-4443.2001 (2001).
691 25 Gallagher, T. M. & Buchmeier, M. J. Coronavirus spike proteins in viral entry and pathogenesis.
692 *Virology* **279**, 371-374, doi:10.1006/viro.2000.0757S0042-6822(00)90757-8 [pii] (2001).
693 26 Letko, M., Marzi, A. & Munster, V. Functional assessment of cell entry and receptor usage for
694 SARS-CoV-2 and other lineage B betacoronaviruses. *Nat Microbiol* **10.1038/s41564-020-0688-y**,
695 doi:10.1038/s41564-020-0688-y (2020).
696 27 Li, W. *et al.* Angiotensin-converting enzyme 2 is a functional receptor for the SARS coronavirus.
697 *Nature* **426**, 450-454 (2003).
698 28 Chen, D. *et al.* GILT restricts the cellular entry mediated by the envelope glycoproteins of
699 SARS-CoV, Ebola virus and Lassa fever virus. *Emerg Microbes Infect* **8**, 1511-1523,
700 doi:10.1080/22221751.2019.1677446 (2019).
701 29 Zhao, X. *et al.* Identification of Residues Controlling Restriction versus Enhancing Activities of
702 IFITM Proteins on Entry of Human Coronaviruses. *Journal of virology* **92**,
703 doi:10.1128/JVI.01535-17 (2018).
704 30 Lin, H. X. *et al.* Identification of residues in the receptor-binding domain (RBD) of the spike
705 protein of human coronavirus NL63 that are critical for the RBD-ACE2 receptor interaction. *The*
706 *Journal of general virology* **89**, 1015-1024, doi:10.1099/vir.0.83331-0 (2008).
707 31 Jun Lan, J. G., Jinfang Yu, Sisi Shan, Huan Zhou, Shilong Fan, Qi Zhang, Xuanling Shi, Qisheng
708 Wang, Linqi Zhang, Xinquan Wang. Crystal structure of the 2019-nCoV spike receptor-binding
709 domain bound with the ACE2 receptor. *BioRxiv* **doi: https://doi.org/10.1101/2020.02.19.956235**
710 (2020).
711 32 Yan, R. *et al.* Structural basis for the recognition of the SARS-CoV-2 by full-length human
712 ACE2. *Science* **10.1126/science.abb2762**, doi:10.1126/science.abb2762 (2020).
713 33 Li, F., Li, W., Farzan, M. & Harrison, S. C. Structure of SARS coronavirus spike
714 receptor-binding domain complexed with receptor. *Science* **309**, 1864-1868 (2005).

715 34 Li, W. *et al.* Receptor and viral determinants of SARS-coronavirus adaptation to human ACE2.
716 *EMBO J* **24**, 1634-1643, doi:7600640 [pii]10.1038/sj.emboj.7600640 (2005).
717 35 Li, F. Structure, Function, and Evolution of Coronavirus Spike Proteins. *Annu Rev Virol* **3**,
718 237-261, doi:10.1146/annurev-virology-110615-042301 (2016).
719 36 Perlman, S. & Netland, J. Coronaviruses post-SARS: update on replication and pathogenesis.
720 *Nat Rev Microbiol* **7**, 439-450, doi:10.1038/nrmicro2147 (2009).
721 37 Wei Deng, L. B., Hong Gao, Zhiguang Xiang, Yajin Qu, Zhiqi Song, Shunran Gong, Jiayi Liu,
722 Jiangning Liu, Pin Yu, Feifei Qi, Yanfeng Xu, Fengli Li, Chong Xiao, Qi Lv, Jing Xue, Qiang
723 Wei, Mingya Liu, Guanpeng Wang, Shunyi Wang, Haisheng Yu, Xing Liu, Wenjie Zhao, Yunlin
724 Han, Chuan Qin. Rhesus macaques can be effectively infected with SARS-CoV-2 via ocular
725 conjunctival route. *BioRxiv* **doi: https://doi.org/10.1101/2020.03.13.990036** (2020).
726 38 Jianzhong Shi, Z. W., Gongxun Zhong, Huanliang Yang, Chong Wang, Renqiang Liu, Xijun He,
727 Lei Shuai, Ziruo Sun, Yubo Zhao, Libin Liang, Pengfei Cui, Jinliang Wang, Xianfeng Zhang,
728 Yuntao Guan, Hualan Chen, and Zhigao Bu. Susceptibility of ferrets, cats, dogs, and different
729 domestic animals to SARS-coronavirus-2 *BioRxiv* **doi:**
730 **https://doi.org/10.1101/2020.03.30.015347** (2020).
731 39 Qiang Zhang, H. Z., Kun Huang, Yong Yang, Xianfeng Hui, Jindong Gao, Xinglin He, Chengfei
732 Li, Wenxiao Gong, Yufei Zhang, Cheng Peng, Xiaoxiao Gao, Huanchun Chen, Zhong Zou,
733 Zhengli Shi, Meilin Jin. SARS-CoV-2 neutralizing serum antibodies in cats: a serological
734 investigation. *BioRxiv* **doi: https://doi.org/10.1101/2020.04.01.021196** (2020).
735 40 Martina, B. E. *et al.* Virology: SARS virus infection of cats and ferrets. *Nature* **425**, 915 (2003).
736 41 Qin, C. *et al.* An animal model of SARS produced by infection of Macaca mulatta with SARS
737 coronavirus. *J Pathol* **206**, 251-259 (2005).
738 42 Rowe, T. *et al.* Macaque model for severe acute respiratory syndrome. *J Virol* **78**, 11401-11404
739 (2004).
740 43 Roberts, A. *et al.* Animal models and vaccines for SARS-CoV infection. *Virus Res* **133**, 20-32,
741 doi:10.1016/j.virusres.2007.03.025 (2008).
742 44 Follis, K. E., York, J. & Nunberg, J. H. Furin cleavage of the SARS coronavirus spike
743 glycoprotein enhances cell-cell fusion but does not affect virion entry. *Virology* **350**, 358-369
744 (2006).
745 45 Thomas HC Sit, C. J. B., Sin Ming Ip, Karina WS Tam, Pierra YT Law, Esther MW To, Veronica
746 YT Yu, Leslie D Sims, Dominic NC Tsang, Daniel KW Chu, Ranawaka APM Perera, Leo LM
747 Poon, Malik Peiris. Canine SARS-CoV-2 infection. *Research Square*
748 **DOI:10.21203/rs.3.rs-18713/v1** (2020).
749 46 Lun, Z. R. & Qu, L. H. Animal-to-human SARS-associated coronavirus transmission? *Emerg*
750 *Infect Dis* **10**, 959, doi:10.3201/eid1005.040022 (2004).
751 47 Safronetz, D., Geisbert, T. W. & Feldmann, H. Animal models for highly pathogenic emerging
752 viruses. *Curr Opin Virol* **3**, 205-209, doi:10.1016/j.coviro.2013.01.001 (2013).
753 48 Linlin Bao, W. D., Baoying Huang, Hong Gao, Lili Ren, Qiang Wei, Pin Yu, Yanfeng Xu,
754 Jiangning Liu, Feifei Qi, Yajin Qu, Wenling Wang, Fengdi Li, Qi Lv, Jing Xue, Shuran Gong,
755 Mingya Liu, Guanpeng Wang, Shunyi Wang, Linna Zhao, Peipei Liu, Li Zhao, Fei Ye, Huijuan
756 Wang, Weimin Zhou, Na Zhu, Wei Zhen, Xiaojuan Zhang, Zhiqi Song, Li Guo, Lan Chen,
757 Conghui Wang, Ying Wang, Xinming Wang, Yan Xiao, Qiangming Sun, Hongqi Liu, Fanli Zhu,
758 Chunxia Ma, Lingmei Yan, Mengli Yang, Jun Han, Wenbo Xu, Wenjie Tan, Xiaozhong Peng, Qi
759 Jin, Guizhen Wu, Chuan Qin. The Pathogenicity of 2019 Novel Coronavirus in hACE2

760 Transgenic Mice. *BioRxiv* **doi: https://doi.org/10.1101/2020.02.07.939389** (2020).
761 49 McCray, P. B., Jr. *et al.* Lethal infection of K18-hACE2 mice infected with severe acute
762 respiratory syndrome coronavirus. *Journal of virology* **81**, 813-821, doi:10.1128/JVI.02012-06
763 (2007).
764 50 Huang, C. *et al.* Clinical features of patients infected with 2019 novel coronavirus in Wuhan,
765 China. *Lancet* **10.1016/S0140-6736(20)30183-5**, doi:10.1016/S0140-6736(20)30183-5 (2020).
766 51 Callaway, E. Labs rush to study coronavirus in transgenic animals - some are in short supply.
767 *Nature* **579**, 183, doi:10.1038/d41586-020-00698-x (2020).
768 52 Day, C. W. *et al.* A new mouse-adapted strain of SARS-CoV as a lethal model for evaluating
769 antiviral agents in vitro and in vivo. *Virology* **395**, 210-222, doi:10.1016/j.virol.2009.09.023
770 (2009).
771 53 Roberts, A. *et al.* A mouse-adapted SARS-coronavirus causes disease and mortality in BALB/c
772 mice. *PLoS Pathog* **3**, e5, doi:10.1371/journal.ppat.0030005 (2007).
773 54 Jiang, D. *et al.* Identification of three interferon-inducible cellular enzymes that inhibit the
774 replication of hepatitis C virus. *J Virol* **82**, 1665-1678, doi:JVI.02113-07
775 [pii]10.1128/JVI.02113-07 (2008).
776 55 Li, W. *et al.* Efficient replication of severe acute respiratory syndrome coronavirus in mouse
777 cells is limited by murine angiotensin-converting enzyme 2. *J Virol* **78**, 11429-11433 (2004).
778 56 Babcock, G. J., Esshaki, D. J., Thomas, W. D., Jr. & Ambrosino, D. M. Amino acids 270 to 510
779 of the severe acute respiratory syndrome coronavirus spike protein are required for interaction
780 with receptor. *J Virol* **78**, 4552-4560 (2004).
781 57 Lin, H. X. *et al.* Identification of residues in the receptor-binding domain (RBD) of the spike
782 protein of human coronavirus NL63 that are critical for the RBD-ACE2 receptor interaction. *J*
783 *Gen Virol* **89**, 1015-1024, doi:10.1099/vir.0.83331-0 (2008).
784 58 Thompson, J. D., Higgins, D. G. & Gibson, T. J. CLUSTAL W: improving the sensitivity of
785 progressive multiple sequence alignment through sequence weighting, position-specific gap
786 penalties and weight matrix choice. *Nucleic Acids Res* **22**, 4673-4680 (1994).
787 59 Kelley, L. A., Mezulis, S., Yates, C. M., Wass, M. N. & Sternberg, M. J. The Phyre2 web portal
788 for protein modeling, prediction and analysis. *Nat Protoc* **10**, 845-858,
789 doi:10.1038/nprot.2015.053 (2015).

790

791

792

793

794

795

796

797